Seismic wave detectability on Venus using ground deformation sensors, infrasound sensors on balloons and airglow imagers

Raphael F. Garcia[1], Iris van Zelst[2,3], Taichi Kawamura[4], Sven Peter Näsholm[5,6], Anna Horleston[7], Sara Klaasen[8], Maxence Lefèvre[9], Celine Marie Solberg[5], Krystyna T. Smolinski[8], Ana-Catalina Plesa[2], Quentin Brissaud[6], Julia S. Maia[2], Simon C. Stähler[8], Philippe Lognonné[4], Mark Panning[10], Anna Gülcher[10,11], Richard Ghail[12], Barbara De Toffoli[13,14]

[1]Institut Supérieur de l'Aéronautique et de l'Espace ISAE-SUPAERO, Université de Toulouse
[2]Institute of Planetary Research, German Aerospace Center (DLR), Berlin, Germany
[3]Centre of Astronomy and Astrophysics, Technical University of Berlin, Berlin, Germany
[4]Université Paris Cité, Institut de physique du globe de Paris, CNRS, Paris, France
[5]Department of Informatics, University of Oslo, Oslo, Norway
[6]NORSAR, Kjeller, Norway
[7]School of Earth Sciences, University of Bristol, Bristol, UK
[8]ETH Zürich, Switzerland
[9]LATMOS/IPSL, Sorbonne Université, UVSQ Université Paris-Saclay, CNRS, Paris, France
[10]Jet Propulsion Laboratory, California Institute of Technology, Pasadena, USA
[11]Seismological Laboratory, California Institute of Technology, Pasadena, USA
[12]Royal Holloway, University of London, London, UK
[13]INAF, Istituto di Astrofisica e Planetologia Spaziali, Rome, Italy
[14]Department of Geosciences, University of Padova, Padova, Italy

Key Points:

- The capabilities of various measurement concepts to detect quakes on Venus are estimated and compared to recent Venus seismicity estimates
- Ground sensors are limited by their short measurement duration, but also by a minimum noise level that may be below atmosphere induced noise
- Atmospheric seismology concepts are limited to large quake magnitudes, and airglow imagers are favored relative to balloon measurements

Corresponding author: Raphaël F. Garcia, raphael.garcia@isae-supaero.fr

Abstract

The relatively unconstrained internal structure of Venus is a missing piece in our understanding of the Solar System formation and evolution. To determine the seismic structure of Venus' interior, the detection of seismic waves generated by venusquakes is crucial, as recently shown by the new seismic and geodetic constraints on Mars' interior obtained by the InSight mission. In the next decades multiple missions will fly to Venus to explore its tectonic and volcanic activity, but they will not be able to conclusively report on seismicity or detect actual seismic waves. Looking towards the next fleet of Venus missions in the future, various concepts to measure seismic waves have already been explored in the past decades. These detection methods include typical geophysical ground sensors already deployed on Earth, the Moon, and Mars; pressure sensors on balloons; and airglow imagers on orbiters to detect ground motion, the infrasound signals generated by seismic waves, and the corresponding airglow variations in the upper atmosphere. Here, we provide a first comparison between the detection capabilities of these different measurement techniques and recent estimates of Venus' seismic activity. In addition, we discuss the performance requirements and measurement durations required to detect seismic waves with the various detection methods. As such, our study clearly presents the advantages and limitations of the different seismic wave detection techniques and can be used to drive the design of future mission concepts aiming to study the seismicity of Venus.

Plain Language Summary

We do not really know what the interior of Venus looks like. Even the first-order structure of the size of Venus' core is plagued with large uncertainties. For other planets, such as the Earth and Mars, the interior structure is much better constrained. This is largely thanks to the seismological investigations performed on these planets that revealed their interior structure by studying the seismic waves caused by quakes. In the next decades, new missions will fly to Venus to explore its tectonic and volcanic activity, but they will not be able to detect any seismic waves. In order to help design future mission concepts, we discuss instruments that could record seismic waves, as already used on the Earth, the Moon, and Mars; instruments on balloons that could float in the Venusian atmosphere; and instruments on spacecrafts that monitor the variations of atmospheric emissions caused by seismic waves originating at the surface. We compare all these different techniques with each other and with recent estimates of Venus' seismic activity to see which of them works best in different scenarios.

1 Introduction

The internal structures of the planets are key information to better understand the formation and the evolution of our Solar System. Although Venus is similar to Earth in terms of size and mass, our knowledge of its internal structure is limited due to its slow rotation, which hinders the determination of its moment of inertia (Margot et al., 2021) and creates large error bars on Love number estimates (Dumoulin et al., 2017). The detection and characterization of seismic waves is the best tool to infer the internal structure of planets (Lognonné et al., 2023). However, the deployment of long-duration geophysical instrumentation, which demonstrated its capabilities during the InSight mission on Mars (Stähler et al., 2021; Durán, Khan, Ceylan, Zenhäusern, et al., 2022; Durán, Khan, Ceylan, Charalambous, et al., 2022; Drilleau et al., 2022; Samuel et al., 2023; Lognonné et al., 2023) is not possible on Venus due to its harsh surface conditions. At the same time, there is a growing number of studies that have presented evidence that Venus is volcanically and tectonically active at present (Smrekar et al., 2010; Gülcher et al., 2020; Byrne et al., 2021; Van Zelst, 2022; Smrekar et al., 2023; Herrick & Hensley, 2023) indicating that the planet is probably also seismically active. Indeed, recent estimates of

Venus' seismicity indicate that Venus could host hundreds of quakes per year with $M_w \geq 5$ when Venus is assumed to be moderately active and potentially be as seismically active as the Earth in its most extreme end-member scenario (Van Zelst et al., 2024).

Despite the compelling arguments in favor of monitoring seismic wave propagation in Venus, none of the three missions scheduled by ESA and NASA to visit Venus in the next decade (i.e., the EnVision (Widemann et al., 2022), VERITAS (Smrekar et al., 2022), and DAVINCI+ (Garvin et al., 2022) missions) are targeting the detection of seismic waves. This is primarily due to the challenges associated with conducting such measurements for Venus. Over the past decade, various measurement concepts have been explored, falling into three main categories: (i) ground deformation instruments deployed on the planet's surface, (ii) infrasound sensors mounted on balloon platforms, and (iii) airglow imagers on board orbiters (Stevenson et al., 2015). The concepts for ground surface deployment of seismic sensors are limited by the high atmospheric surface temperature (≈740 K) in the absence of high temperature electronics. This limits the measurement duration to a total amount of approximately one day (Kremic et al., 2020). Seismic infrasound detection methods concern themselves with the low attenuation of upward-propagating infrasound waves created by seismic waves below 1 Hz (Garcia et al., 2005). These infrasounds conserve the dispersion features of seismic surface waves during their upward propagation (Lognonné et al., 2016). These two properties allow us to assume that the infrasound created by seismic surface waves retains all the properties of seismic surface waves that are necessary to determine the seismic velocity profile in the first hundreds of kilometers depth of the planet, as it was done by InSight on Mars (Kim et al., 2022; Carrasco et al., 2023; Xu et al., 2023). Two different concepts based on the detection of seismic infrasound have been investigated thoroughly in the past decade. First, pressure sensors on board of balloon platforms have been studied (Stevenson et al., 2015; Krishnamoorthy & Bowman, 2023). Their capabilities to detect and characterise seismic waves have been demonstrated theoretically and have even been observed on Earth recently for the first time (Brissaud et al., 2021; Garcia et al., 2022). Secondly, airglow emission variations induced by seismically generated tsunami waves have been observed on Earth (Makela et al., 2011; Occhipinti et al., 2011) and the sensitivity of airglow emissions to gravity waves has been observed in Venus atmosphere (Garcia et al., 2009). Indeed, mission concepts targeted to the observation of seismically-induced variations of 1.27 μm nightglow and 4.3 μm dayglow in Venus' atmosphere have been developed (Stevenson et al., 2015; Sutin et al., 2018).

The purpose of this study is to perform a first comparison between the capabilities of all these diverse measurement techniques and the most recent estimates of Venus seismicity. For each observation technique, we also discuss the minimum performance and measurement duration. We focus on globally observable seismic waves for events of moment magnitude larger than 3 ($M_{\mathrm{W}} > 3$).

2 Estimating seismic wave detection capabilities of different observation concepts

2.1 Seismic signal estimates

In the absence of internal structure models of Venus that are directly constrained by data, the currently-used internal structure models of Venus are constrained by planetary formation and geodynamic models, solar abundance estimates, and physical assumptions, and rely on the adaptation of Earth models to Venus conditions (Zharkov, 1983; Gudkova & Zharkov, 2020). As a consequence, these models present a large uncertainty in terms of both seismic velocities and seismic attenuation parameters. This is why we choose to base our estimates of seismic wave amplitudes and frequency content on Earth's scaling relations, rather than performing complex computations in highly uncertain models of the Venusian interior. Because seismic surface waves show the highest amplitude

for shallow quakes on Earth, we will assume that these waves are also dominating the seismic signal on Venus in the quake magnitude range considered in this study, i.e., moment magnitudes larger than 3.0. In addition, since the dispersion of seismic surface waves is strongly dependent on the seismic structure of the crust and the top of the mantle, the observation of these waves is critical to constrain the structure of the first hundreds of kilometers of Venus' interior. The definition of surface-wave magnitude, M_S, shows a direct link with the amplitude of the seismic surface Rayleigh waves around the 20 s period:

$$M_S = \log_{10}\left(\frac{A_d}{T_S}\right) + 1.66\log_{10}(\Delta) + 3.3, \quad (1)$$

where M_S is the surface wave magnitude, A_d the vertical ground displacement in μm, T_S is the period considered for measuring A_d, and Δ is the epicentral distance of the quake in degrees (Bormann & Dewey, 2012). We will use this relation to determine the amplitude of the surface Rayleigh waves as a function of distance for a given surface wave magnitude.

2.2 Atmosphere effects and parameters

The detectability of infrasound by balloon platforms and airglow imagers is sensitive to the amplitude of the source and atmospheric path effects (Garcia et al., 2005). In particular, attenuation processes on Venus can strongly dampen and disperse the infrasound energy. To assess the impact of attenuation on acoustic waves, we determine the energy loss vs. altitude for a vertically propagating planar wave. In the frequency range of interest (0.01–1 Hz), the attenuation of infrasound in the Venusian atmosphere is dominated by CO_2 relaxation effects (Bass & Chambers, 2001; Petculescu, 2016), although some contributions are also expected from sulfuric acid (H_2SO_4) droplet-related processes, primarily in the cloudy 45 to 70 km altitude regime (Trahan & Petculescu, 2020).

We compute atmospheric parameters using the Venus Climate Database (VCD) (Gilli et al., 2017, 2021; Martinez et al., 2023) to estimate the attenuation due to CO_2 relaxation, $\alpha_{CO2}(z)$. We extract a single vertical profile of specific heats, and sound speed is extracted at the equator at midday local time. From this VCD profile, we then use the approach described in Garcia et al. (2017) to extract the CO_2 relaxation frequency and relaxation strength, as well as the sound speed as a function of altitude. In low-attenuation scenarios, it is appropriate to sum the attenuation contributions from CO_2 and H_2SO_4 (Nachman et al., 1990), to obtain the total attenuation $\alpha_{tot}(z) = \alpha_{CO2}(z) + \alpha_{H2SO4}(z)$. In Figure 1, we use these estimates to explore the amplitude loss using a plane-wave assumption, focusing on acoustic waves at periods from 1 to 50 s from the ground up to 140 km altitude. A significant increase in attenuation occurs in the cloud layers, where strong diffusion-mediated phase changes occur due to sulfuric acid droplets (Petculescu, 2016). Yet, our estimates suggest that attenuation has an insignificant impact on acoustic waves of periods larger than 1 second up to the bottom of the airglow layer IR1. At the altitude of airglow layer IR2, longer-period waves of interest for airglow (10 s to 50 s period) are not damped much. However, at this altitude, a significant energy loss of ∼50% is predicted, which dramatically reduces the likelihood of detection for 1 s period waves. Note that this analysis assumes linear acoustics and takes neither nonlinear propagation nor wave-breaking effects into account.

2.3 Estimating the minimum number of events per magnitude per year

In this section, we provide detection thresholds that can be directly compared to seismicity estimates (Van Zelst et al., 2024). To do so, we estimate the requirements to detect at least one event larger than a given magnitude during the full mission duration.

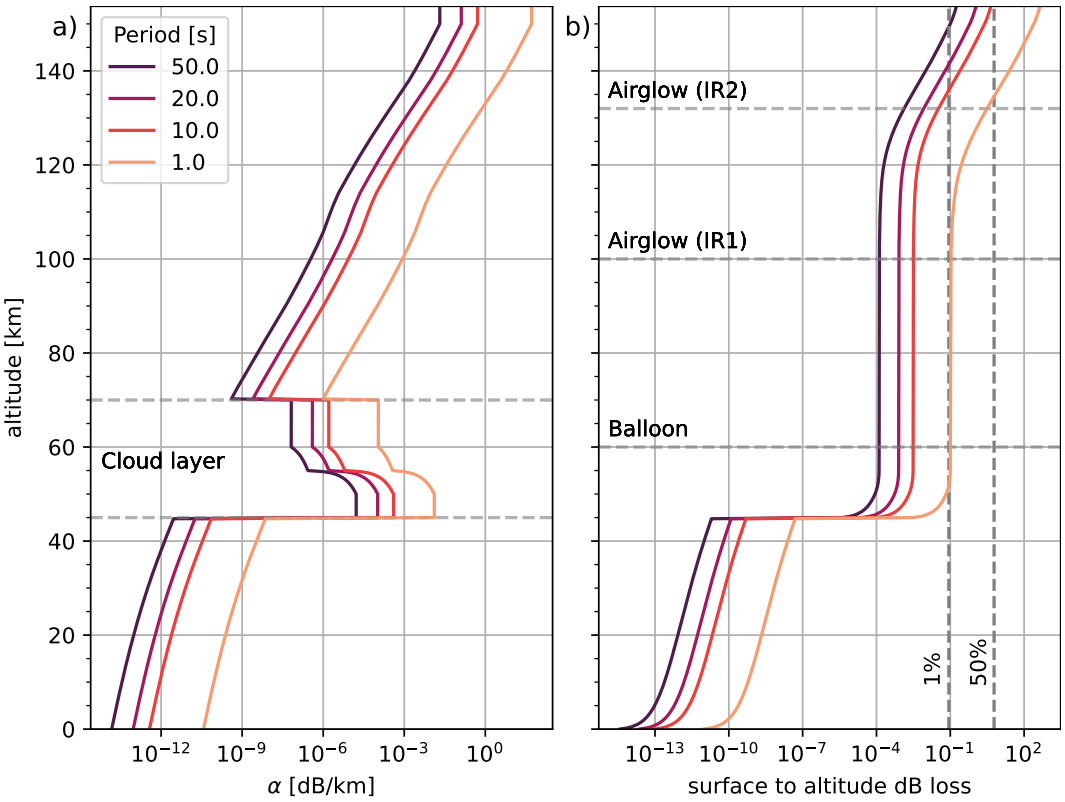

Figure 1. (a) plane-wave infrasound attenuation (α in dB/km) based on a Venus Climate Database (VCD) atmospheric profile, including both the α_{H2SO4} and the α_{CO2} contributions, and the sulfuric acid cloud contributions given in Trahan and Petculescu (2020). We consider wave periods from 1 to 50 s. (b) The total loss (in dB) due to the attenuation in (a), integrated from the ground up to the given altitude. The two vertical dashed lines indicate accumulated amplitude losses of 1% and 50%.

Assuming the seismic events to be Poisson distributed and setting our desired probability of detection at 63% yields the following relation for a signal-to-noise ratio threshold of one:

$$N_m^{\min}(M_S) = \frac{1}{T_m} \frac{S_P}{S_m(M_S)}, \tag{2}$$

where T_m is time in Earth years, S_P is the surface area of Venus, and $*_m$ signifies method m: s for seismometer, r for ground rotation sensor, d for ground Distributed Acoustic Sensing (DAS), b for pressure sensors on board balloons and a for airglow imagers. Using this relation, the surface area $S_m(M_S)$ over which a quake of a given surface-wave magnitude M_S can be detected by a given method is investigated in the following sections.

This relation is only valid statistically with a 63% confidence interval if we assume that the seismic events have a Poisson distribution. Moreover, it is assumed that the seismic event probability is homogeneous over the Venus surface, which is unrealistic, but a starting point at a time when no actual mission concept is evaluated. Our estimates thus provide a lower bound of the detection limits of each measurement concept.

In order to estimate $\frac{S_P}{S_m(M_S)}$, we need to estimate a maximum distance $\Delta_m(M_S)$, usually in degrees, at which the event can be detected for the different methods, within a signal-to-noise ratio larger than a given value $\mathrm{SNR}_{\mathrm{min}}$. Knowing this number, the surface area ratio is

$$\frac{S_P}{S_m(M_S)} = \frac{4\pi}{2\pi(1-\cos(\Delta_m(M_S)))}, \tag{3}$$

with $\Delta_m(M_S)$ the maximum epicentral distance at which you can expect to detect the quake.

Usually, the noise levels of the instruments are provided in Power of Amplitude Spectral Density (ASD) in physical unit over square root of hertz (ASD_n). In contrast, the signal amplitude terms in Equation 1 are provided at a given period (T_S), and consequently the signal amplitude on the instrument is also in physical units at a given period (A_m). In order to compare these two numbers, we convert the amplitude spectral density values into root-mean-square values, under the conservative hypothesis that we filter the signals over a bandwidth of 1/3 octave ($\pm 11.5\%$) around the central frequency $f_S = \frac{1}{T_S}$. As a consequence, the root-mean-square noise amplitude is defined by the product of the amplitude spectral density times the square root of the frequency bandwidth, assuming that the noise power is constant over the bandwidth (Bormann, 2002):

$$N_{\mathrm{rms}} = \mathrm{ASD}_n \sqrt{\frac{0.23}{T_S}}. \tag{4}$$

As a consequence, the maximum epicentral distance at which you can expect to detect a quake of magnitude M_S ($\Delta_m(M_S)$) is defined by equating the signal-to-noise ratio to its minimum value $\mathrm{SNR}_{\mathrm{min}}$, fixed here to 3:

$$\frac{A_m(\Delta_m(M_S))}{N_{\mathrm{rms}}} = \mathrm{SNR}_{\mathrm{min}}. \tag{5}$$

In conclusion, in order to estimate $N_m^{\mathrm{min}}(M_S)$, i.e., the minimum number of events per year, as a function of surface wave magnitude, to measure at least 1 event of this type by a given method, one needs to invert the above equations to get the maximum distance at which an event can be detected by a given method $\Delta_m(M_S)$, and then compute $N_m^{\mathrm{min}}(M_S)$ through Equations 3 and 2. However, because the relation of Equation 1 holds only for teleseismic distances, and because we need the waves to be separated in time in order to analyze them properly, we impose $\Delta_m(M_S) > 3°$. This restriction sets the lower-bound limit on the M_S values.

2.4 Detection capabilities of various observation concepts

2.4.1 Quake detection by landed seismometer

Due to the high surface temperatures on Venus and the limited amount of solar energy that reaches the surface, deploying instruments on the ground is challenging. With conventional electronics, surface landers lasted less than two hours on the Venusian surface in the past (Kerzhanovich & Marov, 1983; Moroz, 1983). However, to be able to determine global seismicity levels, several Earth days of active monitoring would probably be required at minimum.

Recent advances in high-temperature electronics (Wilson et al., 2016; Kremic et al., 2020; Glass et al., 2020) have made long-lived landers a possibility for the coming decades, using silicon carbide (SiC) seismometers. These SiC integrated circuits have been demonstrated to provide 60 functioning days in high-fidelity simulated Venusian surface conditions (Hunter et al., 2021; Chen et al., 2019; Neudeck et al., 2018). However, the

development of the associated electronics coping with the harsh Venus conditions is still required.

Memory is another issue with Venusian surface conditions. Depending on power availability, data storage and transmission could be difficult. Tian et al. (2023) designed a low-memory algorithm to circumvent this issue that triggers transmission during earthquakes and avoids transmission during wind and other noise events (Tian et al., 2023).

Only a handful of probes recorded data at the surface of Venus. Only VENERA-9 and 10 directly measured the wind for 49 min and 90 s, respectively (Avduevskii et al., 1977), and VENERA-13 and 14 indirectly measured the wind speed (Ksanfomaliti et al., 1983). The amplitudes of the measured wind speeds are less than 2 m s^{-1} below 100 m height (Lorenz, 2016), with a higher probability for values below 0.5 m s^{-1}.

Simulations with a global circulation model showed the diurnal cycle of the Planetary Boundary Layer (PBL) activity is correlated with the diurnal cycle of surface winds (Lebonnois et al., 2018), with downward katabatic winds at night and upward anabatic winds during the day along the slopes of high-elevation terrains. With a high-resolution model, Lefèvre et al. (2024) confirmed this diurnal cycle of the surface wind. The resolved large-scale horizontal wind at 10 m above the local surface is above 1 m s^{-1} in the mountains in the equatorial region and below 0.5 m s^{-1} in the low plains.

Lefèvre (2022) used a turbulent-resolving model to quantify the turbulent activity at the surface of Venus. At noon, the height of the PBL varies from 1.5 km in the plains to 7 km in the high terrains by the equator. This difference is due to the impact of the anabatic winds. This difference in PBL height at noon, results in a difference in turbulent horizontal winds amplitude, reaching 2 m s^{-1} for the high terrain compared to between 1 and 1.5 m s^{-1} in the plains. At night, when the impact of the slope winds is weaker, the height of the PBL is almost the same around 500 m, resulting in horizontal winds amplitude below 0.5 m s^{-1}. Placing a seismometer in the low plain, and recording signals by night, seems to be the optimal plan to limit the noise of the atmosphere.

Lorenz (2012) roughly quantified the wind noise at the surface of Venus. With an atmospheric density of 65 kg/m^3, a wind speed of 0.25 m s^{-1} is comparable in terms of dynamic pressure to wind speeds of 20 m s^{-1} on Mars, which were regularly observed during the daytime by InSight (Banfield et al., 2020) The corresponding seismic amplitude is 120.0 nm. Atmospheric noise could therefore limit seismic detection, and shielding the instrument might be necessary.

Venera-14 reportedly detected Venusian microseisms with a geophone in only an hour of operation (Ksanfomaliti et al., 1982). The amplitude of the signals are consistent with 'noisy' environments on Earth (Lorenz & Panning, 2018), i.e. from $\sim 10^{-8}$ to 10^{-6} $m/s^2/\sqrt{Hz}$ which roughly spans the space between the low and high noise models for Earth (Peterson, 1993). Therefore, surface-wind noise on Venus must be properly quantified. In addition, it is important to note that for high-quality seismic measurements, the wind speed and pressure should be monitored continuously.

The Brownian noise of a Short Period (SP) sensor comparable to the InSight sensor (Lognonné et al., 2019) in a vacuum is modeled to have an acceleration noise density of $\sqrt{\frac{k_B T \alpha}{m}}$ where k_B is Boltzmann's constant, T the absolute temperate, α the damping constant, and m the proof mass (Mimoun et al., 2017). For a standard SP, the proof mass is 0.8 g. Recalculating from Mimoun et al. (2017) with $T = 740$ K, gives a noise of $4.37 \cdot 10^{-10}$ $m/s^2/\sqrt{Hz}$. If not in a vacuum, the suspension noise also includes a viscous damping term which could contribute. At 740 K, this additional term reaches $3.3 \cdot 10^{-9}$ $m/s^2/\sqrt{Hz}$, giving a total suspension noise of $3.77 \cdot 10^{-9}$ $m/s^2/\sqrt{Hz}$, lower than the atmospheric noise. Other sensor noise sources should also be considered and properly calculated for the Venusian environment, such as digitizer/acquisition noise, ther-

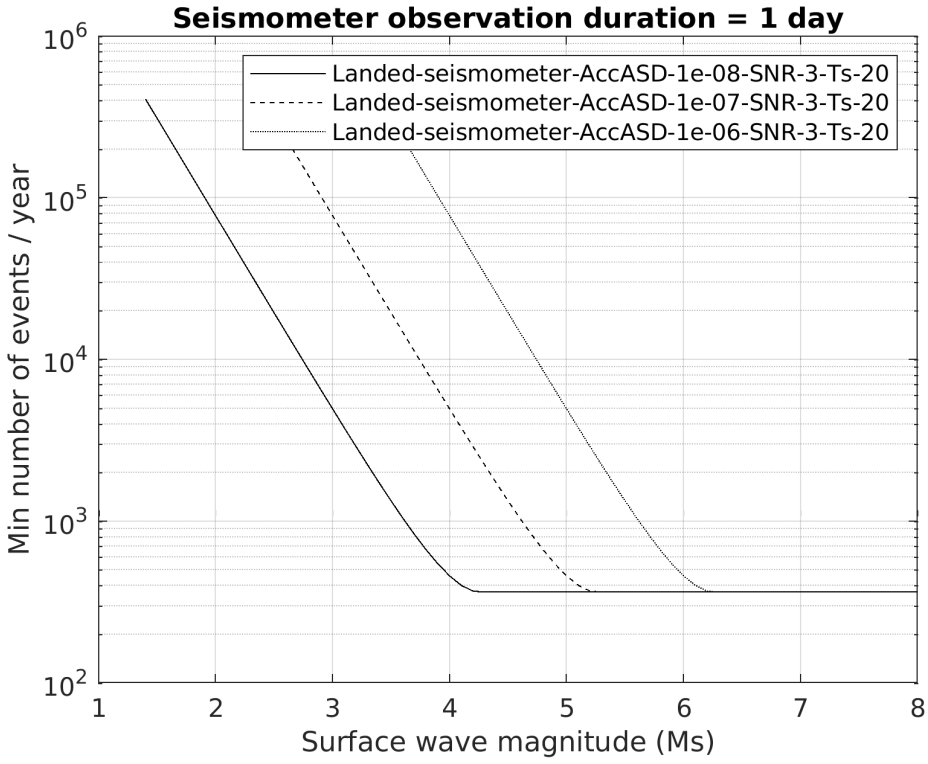

Figure 2. Minimum number of events per year as a function of surface wave magnitude required on the surface of Venus to measure at least one event of this magnitude during a seismometer observation duration of 1 day. Results are provided for different noise levels: 10^{-8} (plain line) and 10^{-7} (dashed line), 10^{-6} (dotted line) $\mathrm{m/s^{-2}}/\sqrt{\mathrm{Hz}}$ at 20 s period.

mal noise, noise from wind on the sensor, and atmospheric noise/noise of the lander itself.

With an SNR_{min} set to 3 and a period T_s of 20 s, $\Delta_m(M_\mathrm{S})$ can be estimated for a given magnitude from Equations 1 and 5 as:

$$\log_{10}\left(\Delta_m(M_\mathrm{S})\right) = \frac{M_s - 3.3 - \log_{10}\left(\frac{SNR_{min}N_\mathrm{rms}}{T_s}\right)}{1.66}. \tag{6}$$

Following Equations 2 and 3, the minimum number of events for each magnitude on the surface of Venus to result in at least one detection during the mission lifetime is shown in Figure 2. For the lowest noise level estimated to be 10^{-8} $\mathrm{m/s^2}/\sqrt{\mathrm{Hz}}$, global detection is possible for surface wave magnitudes above $M_s = 4.3$. For a higher noise level, this limit increases to $M_s = 5.3$ for $10^{-7}\mathrm{m/s^2}/\sqrt{\mathrm{Hz}}$ and to $M_s = 6.3$ for 10^{-6} $\mathrm{m/s^2}/\sqrt{\mathrm{Hz}}$. Under our idealized conditions, events above this threshold need to occur just once during the mission to be detectable, which creates the lower limit of 365 events per year in fig. 2.

2.4.2 Quake detection with DAS on the surface

Distributed Acoustic Sensing (DAS) is an emerging technology in the field of Earth geophysics, and has been applied in increasingly remote and harsh locations on Earth,

such as glaciers (Walter et al., 2020; Hudson et al., 2021), volcanoes (Klaasen et al., 2021; Jousset et al., 2022; Klaasen et al., 2023) and submarine environments (Cheng et al., 2021; Lior et al., 2021). It employs a fiber-optic cable that is interrogated with laser pulses, resulting in seismic deformation measurements at a high spatial and temporal resolution along the cable. We refer the reader to Zhan (2020), and Lindsey and Martin (2021) for more in-depth descriptions of DAS and its applications on Earth. We optimistically propose to extend the use of DAS beyond Earth, and to visualize the hypothetical detection capabilities of DAS on Venus.

We follow the procedures as outlined in Section 2.3 to obtain the detection capabilities for DAS on Venus, as shown in Figure 3. We estimate the minimum number of required events per year based on parameters and assumptions similar to the ones used for the landed seismometer in Section 2.4.1. On top of the noise estimates of 10^{-8}, 10^{-7} and 10^{-6} $\mathrm{m/s^2/\sqrt{Hz}}$, we also use the noise-floor in strain as reported by the iDAS Carina from Silixa, as an example of the self-noise of an interrogator currently on the market. The noise estimates in $\mathrm{m/s^2/\sqrt{Hz}}$ are transformed from ground acceleration to strain using the plane-wave assumption (Daley et al., 2016; Wang et al., 2018; Näsholm et al., 2022), assuming an apparent velocity of seismic surface waves of 2250 m/s, which corresponds to an approximate Rayleigh wave velocity in mid-oceanic ridge basaltic material at 20 second period (as suggested for Venus; Surkov et al., 1984) with a Poisson ratio of 0.25:

$$\epsilon = aT_\mathrm{S}/V_\mathrm{R}, \tag{7}$$

where ϵ is the strain, a is the acceleration in $\mathrm{m/s^2}$ which is linked to a given quake magnitude by Equation 1, T_S is the period of the wave in s, and V_R is the Rayleigh wave velocity in m/s. The entire calculation is then based on the values in strain; the native unit of a DAS interrogator.

While the calculation based on different noise estimates paints an optimistic picture, we emphasize that a DAS deployment on Venus is at the moment not feasible due to several obstacles, such as (i) the current instrumental capacities, (ii) deployment options, (iii) cable coupling conditions, and (iv) unknown cable locations. The instruments currently on the market are not able to operate under the pressure and temperature at the surface of Venus. However, some experiments have demonstrated the ability of specialized gold-coated optical fibers to survive and function with low attenuation at temperatures up to 773 K for up to 900 hours (Jacobsen et al., 2018), with optical fiber manufacturers also quoting operating temperatures up to 973 K (e.g. (Heracle, 2023)). The development of high-temperature and corrosion-resistant fibers is an area of active research, for example within the oil and gas industry (Reinsch & Henninges, 2010; Stolov & OFS, 2019)). Alternative fiber optic sensing systems are also already in development for structural health monitoring on future spacecraft (Chan et al., 2015; Parker et al., 2024).

Assuming the further development of DAS instruments and their ability to operate on Venus, we are limited by the deployment of the cable. If the cable is released during the landing, we are unable to control the exact layout and coupling conditions of the cable, which will likely decrease the data quality and the consequent conclusions that can be drawn from the data. If the cable is not buried and protected, other noise sources are likely to overpower any seismic signals - a phenomenon observed on Earth with atmospheric noise, in submarine environments with strong currents (Lior et al., 2021), or on Mars with the atmospheric wind and pressure noise (Mimoun et al., 2017). Additionally, DAS yields single-component data, therefore a cable layout with varying angles and directions is necessary to capture the complete wavefield and locate events. However, this also requires exact geographical knowledge of the cable layout, which may be difficult

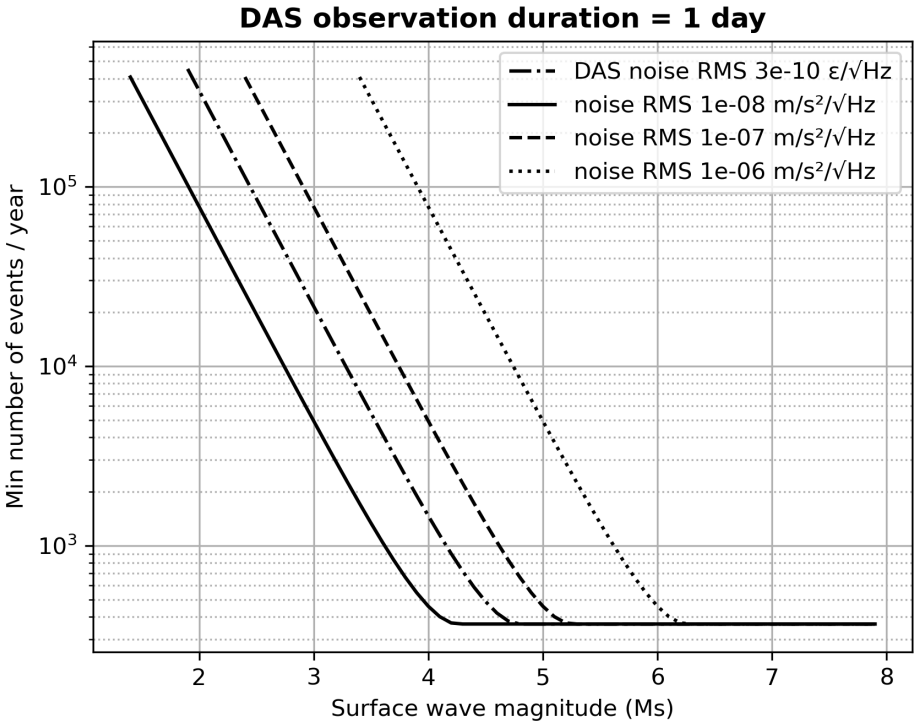

Figure 3. Minimum number of events per year as a function of surface wave magnitude required to measure at least one event of this magnitude during a DAS observation duration of 1 day. Results are provided for different noise levels: 10^{-8} (plain line) and 10^{-7} (dashed line), 10^{-6} (dotted line) $\mathrm{m/s^{-2}/\sqrt{Hz}}$ at 20 s period. An estimate assuming that the noise floor is controlled by a typical self noise of a DAS interrogator (iDAS Carina of Silixa company) is provided as dotted-dashed lines.

to obtain on Venus due to the lack of a GPS network and difficulty capturing georeferenced images of the cable.

Hence, in order to facilitate a DAS experiment on Venus, research primarily needs to focus on instrumental development and the feasibility of experimental deployment. The instrument needs to be able to operate its laser and conduct preliminary data analysis before sending the data back to orbit to avoid, in order to avoid a bottle neck caused by the large amounts of data produced by DAS experiments. Additionally, the cable needs to be deployed in such a fashion to guarantee atmospheric protection and good coupling with the ground, and would ideally have a well-known, and non-linear layout.

2.4.3 Quake detection with ground rotation sensors

The sensing of the ground rotations induced by seismic waves is an emerging field. The ground rotations allow for inferring the gradients of the seismic wavefield. These measurements allow seismologists to distinguish between various seismic waves (Sollberger et al., 2023), to correct for tilt effects on seismometers (Bernauer, Wassermann, & Igel, 2020) and to infer anisotropy parameters (Noe et al., 2022). There are also many other applications for inverse problems and seismic source determination (Schmelzbach et al., 2018). This domain is currently limited by the self-noise level of the instruments (Bernauer

et al., 2021) and planetary applications are promising but mainly limited by the available instrumentation (Bernauer, Garcia, et al., 2020).

The currently available instruments are measuring the ground rotation speed in rad/s (ω) along three perpendicular axis. With the same assumption as those used in the previous section to estimate the ground strain, this parameter can be linked to the ground acceleration by the following equation

$$\omega = aT_S/(2\pi\lambda), \tag{8}$$

where ω is the ground rotation in rad/s, a the acceleration in m/s^2, T_S the period of the surface wave in s, and λ the wavelength in meters which is computed assuming a surface wave velocity of 2250 m/s.

We follow the procedures as outlined in Section 2.3 to obtain the detection capabilities for ground rotation sensors on Venus as shown in Figure 4. We estimate the minimum number of required events per year based on parameters and assumptions similar to the ones used for the landed seismometer in Section 2.4.1. On top of the noise estimates of 10^{-8}, 10^{-7} and 10^{-6} m/s$^2/\sqrt{\text{Hz}}$, we also use the noise-floor in rad/s as reported for the BlueSeis3A sensor from the iXblue company (20 nrad/s/$\sqrt{\text{Hz}}$), as an example of the self-noise of a rotation sensor on the market.

As observed in Figure 4, the event detection is limited by the self-noise of current ground rotation instruments (Bernauer, Garcia, et al., 2020). As a consequence, even if the ground rotation measurements present less deployment constraints than the DAS systems, the interest of such measurements is limited to large-amplitude signals, and thus to large-amplitude quakes close to the instrument.

2.4.4 Quake detection by pressure sensors onboard balloons

Stratospheric balloon flights on Earth present noise levels around 0.05 Pa/$\sqrt{\text{Hz}}$ at 20 s period and 0.01 Pa/$\sqrt{\text{Hz}}$ at 10 s period (Garcia et al., 2022). The amplitude of pressure perturbations generated by a vertical displacement A_d (in µm) at period T_S can be computed using the following formula, assuming that the acoustic wave attenuation is negligible (Garcia et al., 2005):

$$DP = \rho(z_b)c(z_b)\sqrt{\frac{\rho(0)c(0)}{\rho(z_b)c(z_b)}}\left(\frac{10^{-6}2\pi A_d}{T_S}\right) \tag{9}$$

in which $\rho(z)$ and $c(z)$ are the density and the sound speed at altitude z in the atmosphere respectively. The product of the first two terms is the impedance conversion from particle velocity to pressure at balloon altitude (z_b = 60 km). The third term is the amplification factor for particle velocity from the ground to the balloon altitude. The last term is the ground velocity of seismic waves in m/s at T_S period.

Using Equations 2, 3, 6, 5, 4 and 9 one can obtain the minimum number of events per year required to measure at least 1 event of a given magnitude during the observation duration. The results are presented in Figure 5. This suggests a minimum amount of events M_S = 6 between 20 and 100 is required to detect at least one quake. Note that at large magnitudes, the minimum number of events is limited to 4 per year, because the mission duration is 1/4 of a year.

2.4.5 Quake detection by Airglow measurements onboard orbiters

Various studies pointed to the sensitivity of Venus' airglow emissions to pressure, temperature and density variations induced by acoustic waves (Garcia et al., 2009; Stevenson et al., 2015; López-Valverde et al., 2011). These studies mainly target two infrared

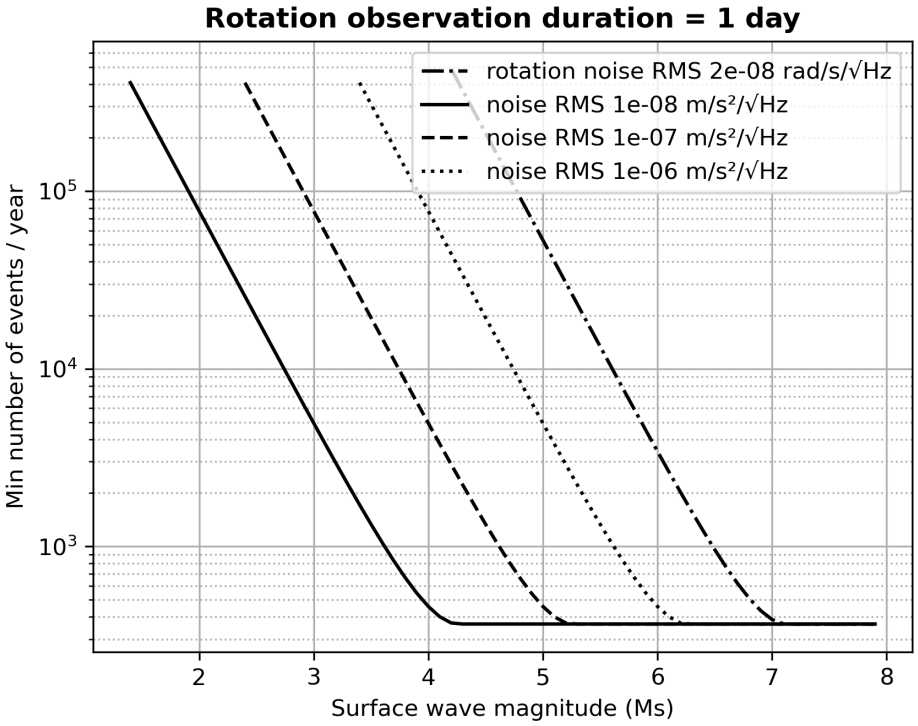

Figure 4. Minimum number of events per year as a function of surface wave magnitude required to measure at least one event of this magnitude during a ground rotation observation duration of 1 day. Results are provided for different noise levels: 10^{-8} (plain line) and 10^{-7} (dashed line), 10^{-6} (dotted line) $\mathrm{m/s^{-2}}/\sqrt{\mathrm{Hz}}$ at 20 s period. An estimate assuming that the noise floor is controlled by a typical self noise of a ground rotation instrument (BlueSeis-3A of iXblue company) is provided as dotted-dashed lines.

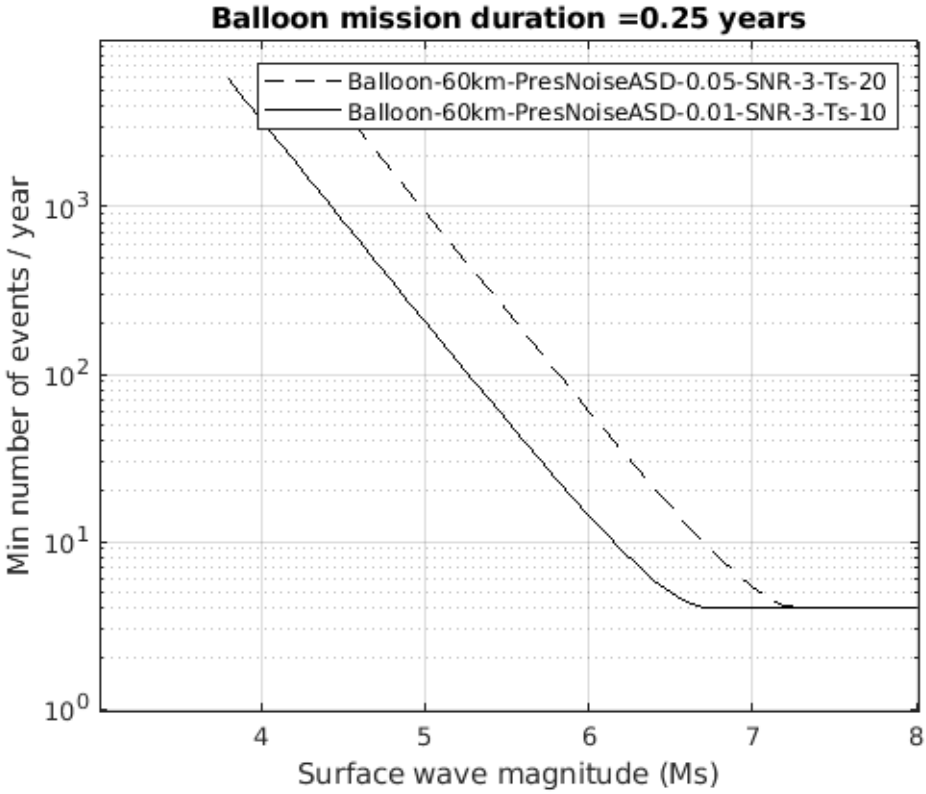

Figure 5. Minimum number of events per year as a function of surface wave magnitude required to measure at least one event of this magnitude during a balloon mission duration of 3 months. Results are provided at two different periods: 20 s (dashed line) and 10 s (plain line) because the noise level of pressure measurements varies significantly with frequency (from 0.05 to 0.01 Pa/$\sqrt{\text{Hz}}$ going from 20 s to 10 s period).

airglows: nighttime airglow at 1.27 μm and day time Non-Local Thermodynamical Equilibrium emissions around 4.3 μm (in fact two emission peaks at 4.28 μm and 4.32 μm). These studies paved the way to a dedicated mission concept studied at JPL/NASA (Sutin et al., 2018). We will use this mission design, called VAMOS, in order to infer the detection capabilities of airglow measurements in terms of the minimum number of events per year required to detect at least one quake with this detection method. The concept is targeting a continuous monitoring of the planet disk with a high sampling rate (> 1 sample per second) camera orbiting on a circular equatorial orbit at a radius of 45,000 km with a period of approximately 29.2 hours.

As the measurement concept is different from a single point measurement by landed seismometers or balloons, Equation 2 must be revised. First, because the airglow emissions are localized only on a specific part of the planet, we must define this area as the Observation Area (OA) for a given airglow. For 1.27 μm emission, this observation area is centered on the equatorial point at 1:00 AM local time and covers an angular radius of about 60° around that point, because it is in this region that we expect the largest background emissions (Gérard et al., 2008). For simplicity, we assume that the center point of this area is located at midnight local time. For 4.3 μm emission, the observation area is centered on the equatorial point at 12:00 local time (midday) and covers an angular radius of about 70° around that point. These emissions are proportional to solar illumination, but polar regions and regions close to the terminator are conservatively excluded because background emissions are low, and because more variability is expected from gravity wave activity (Seiff & Kirk, 1991; Garcia et al., 2009; Gérard et al., 2014).

Then, another difference compared to single point measurements is that the observation area is not always visible in the camera images. To illustrate this, we use the equatorial circular orbit of VAMOS to simplify the computations, although it still provides similar visibility statistics to other orbits at different ellipticity and inclination when ensuring that the full disk is visible on more than 80% of the orbit period. In the full-disk images of the planet, we conservatively consider that only points having an angular distance smaller than 70° for the center of the image (located at the equator) can be used for observation because points close to the limb will have too much image distortion. As a consequence, for a given local time position (ϕ in longitude degrees) of the center of the image (at the equator) relative to the center position of the visibility area (ϕ_0) the visible observation area (VOA) will be defined by the intersection of two spherical caps (or solid angles) of size 60° (or 70°) for the observation area and size 70° for the imaging capability. Due to the rotation of the spacecraft around the planet, the size of the visible observation area will vary as a function of the parameter ϕ.

The function $VOA(\Delta\phi)$, with $\Delta\phi = \phi - \phi_0$ is symmetric around zero. When this area is zero (i.e., the observation area is not visible from the spacecraft) the corresponding time period must be subtracted from the mission duration to define the observation duration (T_m of Equation 2). When this area is non-zero, all the points in the area have the capability of detecting seismic waves. Consequently, the surface $S_m(M_\mathrm{S})$ of Equation 2 is much larger than for a single-point observation because it includes the whole visible observation area $VOA(\Delta\phi)$, and extends it in both latitude and longitude directions by $\Delta_m(M_\mathrm{S})$ degrees. When the surface of the visible observation area is non-zero, the surface of the detection area is computed by the joint area of two spherical caps for each surface wave magnitude (M_S) and each longitude separation ($\Delta\phi$) between the two spherical caps (i.e., the visibility area and the image usable area). The average area over all possible $\Delta\phi$ values is then scaled to 4π as in Equation 2. The observation duration is reduced by the amount of time during which the visible observation area is zero.

Once these geometrical considerations have been taken into account, we still have to compute the maximum distance at which a quake can be observed by a point in the observation area $\Delta_m(M_\mathrm{S})$.

For the 1.27 μm nighttime emissions, we need to convert the vertical particle velocity in the acoustic wave into airglow emission and compare to the instrument noise. The vertical particle velocity at the altitude of the maximum emission rate of the 1.27 μm airglow ($z_{IR1} = 100\ km$) is provided by:

$$A_{\mathrm{v}}(z_{IR1}) = \sqrt{\frac{\rho(0)c(0)}{\rho(z_{IR1})c(z_{IR1})}} \left(\frac{10^{-6} A_{\mathrm{d}}(0)}{2\pi T_{\mathrm{S}}} \right) \tag{10}$$

where $A_{\mathrm{d}}(0)$ as function of surface wave magnitude is provided by inverting Equation 1. The sensitivity of 1.27 μm emissions is driven by the transport of the emitting molecules under the vertical velocity $A_{\mathrm{v}}(z_{IR1})$ (Lognonné et al., 2016). The order of magnitude of this sensitivity is about 3.0%/(m/s) at 20 s period and 6%/(m/s) at 50 s period at 100 km altitude (Sutin et al., 2018) In addition, the estimated noise level of an imaging InfraRed (IR) camera targeting these emissions is about 0.5% of background emission level (Sutin et al., 2018).

For the 4.3 μm daytime emission, we focus on the 4.28 μm emission peak and assume that the emission altitude is approximately 135 km and that these emissions present a sensitivity of 1% per Kelvin variation of atmospheric temperature (López-Valverde et al., 2011). In order to convert the vertical particle velocity $A_v(z_{IR2})$ into temperature perturbation (in Kelvin), we use the impedance at $z_{IR2} = 135$ km altitude:

$$DP(z_{IR2}) = \rho(z_{IR2})c(z_{IR2})A_v(z_{IR2}) \tag{11}$$

$$= \rho(z_{IR2})c(z_{IR2}) \sqrt{\frac{\rho(0)c(0)}{\rho(z_{IR2})c(z_{IR2})}} \left(\frac{10^{-6} 2\pi A_{\mathrm{d}}(0)}{T_{\mathrm{S}}} \right) \tag{12}$$

which is similar to Equation 9 but at the altitude of the 4.28 μm emission peak. Then, we assume both the perfect gas law and the adiabatic nature of the acoustic wave perturbations in order to quantify the corresponding temperature changes through the following equation:

$$DT(z_{IR2}) = \frac{\gamma - 1}{\gamma} \frac{T(z_{IR2})}{P(z_{IR2})} DP(z_{IR2}), \tag{13}$$

where γ is the heat capacity ratio at altitude $z_{IR2} = 135\ km$, and $T(z_{IR2})$ and $P(z_{IR2})$ are the background temperature and pressure at this altitude, respectively. Finally, using the sensitivity of 1% per Kelvin of the 4.28 μm emission, we obtain the expected signal in percentage of background emission (López-Valverde et al., 2011). Concerning the instrument noise, we assume that the root-mean-square noise of the detector is about 0.125% of background emission (Sutin et al., 2018).

Gathering all these equations, we obtain the minimum number of events per year for a mission duration of 2 years, and for the two infrared emissions. This result is shown in Figure 6. The minimum surface magnitude that can be detected through these airglow emissions is between 4.5 and 5. However, we have a low variability of the minimum number of events per year because of the large extent of the observation area.

2.4.6 Comparing the different seismic wave measurements concepts

Figure 7 assembles the detection capabilities of all the different seismic wave measurement concepts in the same figure, although the ground sensors in this figure are limited to seismometers, as the other ground measurement concepts are not yet technologically feasible. From this figure, it is clear that the airglow emissions are best designed to detect quakes of surface wave magnitude larger than 5. In addition, the capability of

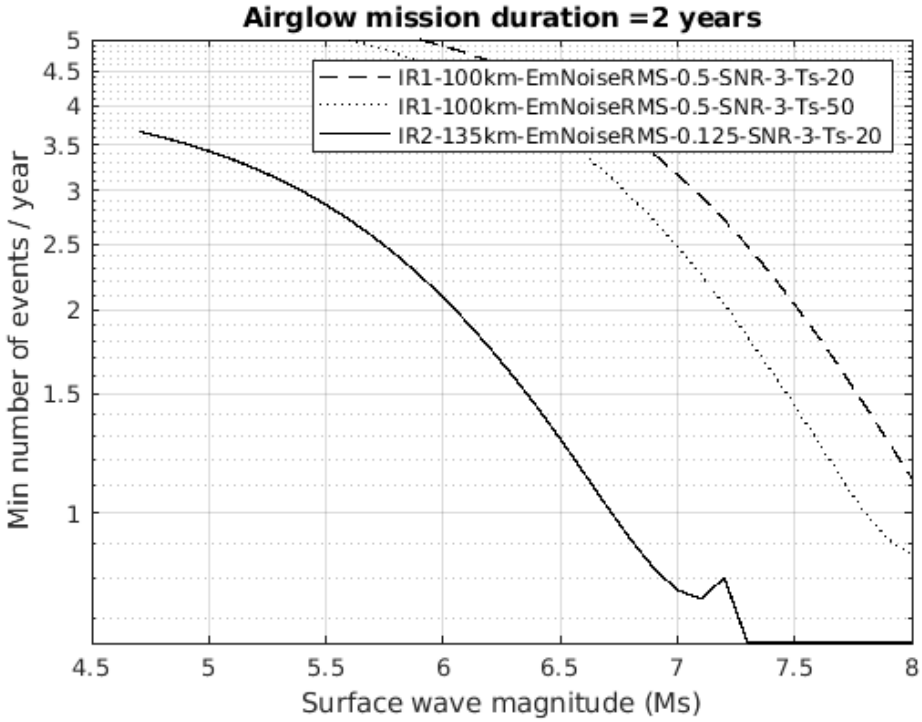

Figure 6. Minimum number of events per year as a function of surface wave magnitude required to measure at least one event of this magnitude during an airglow orbiter mission duration of 2 years. Results are provided for the two airglow emissions respectively at 1.27 µm (dashed line at 20 s period, dotted line at 50 s period) and at 4.28 µm (solid line).

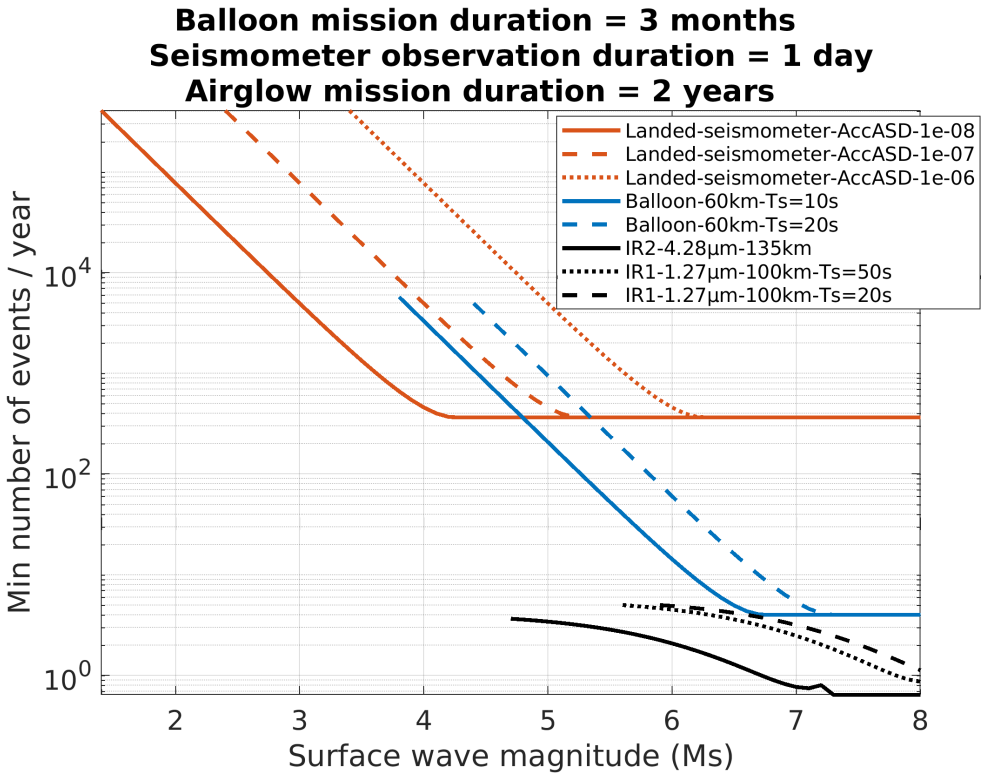

Figure 7. Minimum number of events per year as a function of surface wave magnitude required to measure at least one event of this magnitude for all the detection methods. Balloon estimates in blue, landed seismometers in brown, and airglow emissions in black.

such observations to track surface wave propagation on the images is opening more opportunities to image lateral variations in the crust and the lithosphere. However, due to low-pass effects, induced by the vertical extent of airglow emission peaks and by the response of airglow emissions to acoustic forcing, these observations are probably limited to periods larger than 10 s (Lognonné et al., 2016; Sutin et al., 2018).

The balloon observations have a detection limit around 4.0–4.5 units of surface wave magnitude and can detect all quakes with surface wave magnitude larger than 7. In addition, they can detect higher frequency signals, with a usable bandwidth mainly for periods between 0.5 s and 20 s. However, this observation mean suffers for its single point measurement and from the short mission duration, estimated here to be 3 months.

Finally, for short duration deployment of a landed seismometer, the estimates present a large variability due to the large uncertainties on the final noise level of such an instrument. Assuming a noise level between 10^{-7} and 10^{-6} m/s$^2/\sqrt{\text{Hz}}$ at 20 s period, such an instrument can detect all quakes of surface wave magnitude larger than 5 to 6. In addition, for small quakes close to the sensor, the bandwidth of such an instrument would easily cover the 0.05–20 Hz. However, such a concept is strongly limited by the short observation duration, assumed here to be 1 day, such that it would allow us to investigate only seismic events that are occurring more than 400 times per Earth year.

3 Comparing of detection capabilities with current seismicity estimates

Our estimates of detection capabilities are shown in figure 7 as a function of surface wave magnitude M_S which was defined following the IASPEI standard and corresponds to the definition of M_S_20 by (Bormann et al., 2013). However, seismicity estimates are usually provided as a function of seismic moment magnitude M_W which is a better representation of the quake physics. In order to convert from M_S to M_W, we use the following relation defined by Bormann et al. (2013) for quake moment magnitudes smaller than 6.8 that are of our main interest:

$$M_W = 0.667\ M_S + 2.18 \tag{14}$$

The error bar in this conversion is on the order of 0.3 magnitude unit, but even such large errors could in fact be smaller than the error we may have due to the unknown internal structure of Venus. Eventually, the moment magnitude is converted to the seismic moment M_0 (in Nm) by the standard conversion formula $M_W = \frac{2}{3}(\log_{10}(M_0) - 9.1)$.

Once M_S has been converted into M_W or M_0, we can directly compare our detection limits of at least one quake with a signal-to-noise ratio larger than 3 over the mission duration with the Venus seismicity estimates by (Van Zelst et al., 2024). This comparison is presented in Figure 8.

The detection limits presented here should be taken with caution for two main reasons. First, the limitations presented in the next section induce an error bar on the order of one order of magnitude on these estimates. Secondly, we investigated mainly seismic signals around the 20 s period whereas the expected bandwidths of the different methods are different with an upper bound frequency of 10 Hz for ground sensors to 0.1 Hz for airglow observations.

Despite these limitations, a few interesting observations can be made in Figure 8. The ground-based sensors can be considered adequate for seismic wave detection if their noise level at 20 s period is below 10^{-8} m/s$^2/\sqrt{\text{Hz}}$ and if they are deployed in an active seismic area that would allow us to detect quakes of magnitudes smaller than 4.0. The pressure sensors on balloon platforms allow for probing quake magnitudes in the 5.0 to 7.0 moment magnitude range and mainly for seismic signal frequencies in the 0.05 to 1 Hz range. Lastly, the airglow measurements have the lowest detection limits due to the low noise level and the long duration of the observations. In addition, the output movie of wave propagation would allow for determining the source location and investigating variations in seismic surface speeds over the planet that could be related to lateral heterogeneities in the shallow seismic wave structure of the crust. However, this measurement concept is limited to seismic moment magnitudes larger than 5.5 and to wave periods larger than 5 s.

4 Limitations

Our analysis operated under certain assumptions that leave room for future improvements and exploration.

First, the spatial dependence of seismicity estimates is not taken into account in our estimates of quake detectability, despite the likelihood that certain areas on Venus exhibit higher seismic activity compared to others. Even if this issue is not so critical for airglow measurements that will cover a large part of the planet surface, it is obvious that ground sensor deployments should target the most active regions in order to improve their detection capabilities. The balloon missions are also expected to cover more equatorial regions than polar regions due to deployment and mission duration constraints.

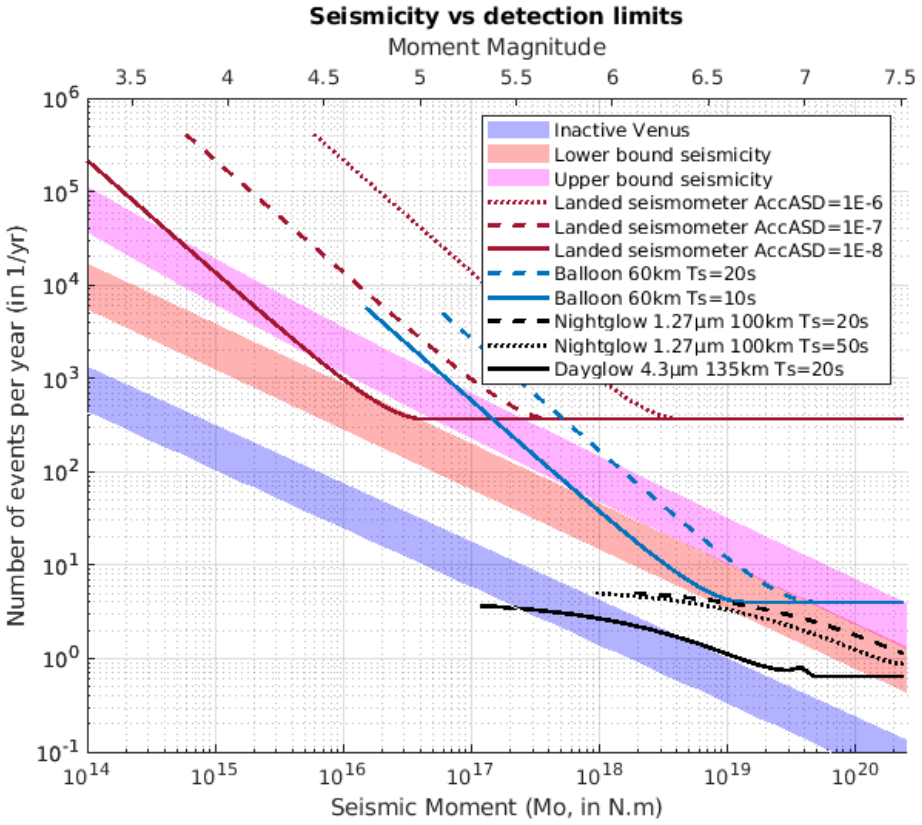

Figure 8. Minimum number of events per year as a function of seismic moment (in N·m) on the bottom and moment magnitude on top required to measure at least one event of this magnitude for all the detection methods (lines) compared to end-member Venus seismicity estimates (shaded areas) by Van Zelst et al. (2024): an inactive Venus (blue), lower bound active Venus (red) and upper bound active Venus (magenta). Balloon estimates are in dark blue, landed seismometers in brown, and airglow emissions in black.

A second important limitation is the uncertainty on the noise levels of each measurement concept. Even though we consider reasonable assumptions on these numbers and provided estimates for different noise levels, detailed noise models of these measurement concepts are required to fully validate our analysis. Mimoun et al. (2017) provides an example of a detailed noise model for a seismometer instrument. An inherent difficulty to the noise model exercise is that the mission parameters (lander size, instrument performance parameters, etc.) must be known in order for the analysis to be valid.

Lastly, the method used to relate ground movements to quake magnitude and the frequencies considered here (periods between 10 and 50 seconds) are mainly relevant for quake moment magnitudes between 4.0 and 6.8 (Bormann et al., 2013). For quake moment magnitudes smaller than 4.0, other methods and frequency ranges should be considered.

5 Conclusion

Our study provides a first estimate of the detection capabilities of long period seismic surface waves on Venus by various measurement concepts: ground sensors including seismometers, DAS, and rotation sensors; infrasound sensors on balloons; and airglow imagers onboard orbiters. We also compare these estimates with recent predictions of Venus seismicity. The airglow measurement concept appears to be most relevant in light of the current estimates of seismicity, but it is limited to moment magnitudes larger than 5.5 and wave periods larger than 5 s. We find that a minimum measurement duration of two years ensures a good probability to detect large magnitude quakes. Infrasound sensors onboard balloons must ensure an overall noise level below 10^{-2} Pa/$\sqrt{\text{Hz}}$ at 10 s period and a measurement duration in the order of a month to obtain a good probability of quake detection. The ground sensors are strongly limited by their measurement duration but also by their noise, mainly due to instrument self-noise for potential ground rotation sensors, and noise induced by the installation or environment for seismometers and potential DAS fiber measurements that would be effective only with an overall acceleration noise level at 20 s period below 10^{-8} m/s^2/$\sqrt{\text{Hz}}$. Uncertainties ranging up to one order of magnitude impact these detection limit estimates due to limitations that could be improved in various directions by future studies. Potential directions of improvements would be to take into account the geographical distribution of quakes, a full modeling of the amplitude of seismic and infrasound waves, detailed noise models of the measurement concepts... Rather than definitively concluding on one measurement concept, our study allows us to enhance the advantages and limitations of each measurement concept and can drive requirements on future mission concepts that would deploy such measurement tools.

Despite the recent selection of various space missions to Venus, none of these will target the detection and characterization of seismic waves to investigate Venus' internal structure in better detail. The most realistic programmatic scenario for the implementation of any of the measurement concepts described in this study in the next decade is therefore the deployment of such concepts by a small satellite as a piggyback payload on one of these missions.

Open Research

All the codes and input data used to create the figures in this article are available at the following zenodo repository https://zenodo.org/records/10943310 (DOI: 10.5281/zenodo.10943310).

Author contributions

Conceptualization: RFG, IvZ, KTS
Data curation:
Formal Analysis: RFG, SK, TK
Funding acquisition: IvZ
Investigation: RFG, SPN, QB
Methodology: RFG, SS
Project administration: IvZ
Resources: ML
Software: RFG, TK, SK, CMS
Supervision:
Validation: SPN, ML, CMS, QB
Visualization: RFG, SK, CMS, SPN
Writing – original draft: RFG, SK, SPN, QB, ML, AH, TK, KTS, CMS
Writing – review & editing: AG, SPN, IvZ, BDT, QB, ML, JM, ACP, AH, SS, PL, MP, KTS

Acknowledgements

This research was supported by the International Space Science Institute (ISSI) in Bern, Switzerland through ISSI International Team project #566: "Seismicity on Venus: Prediction & Detection", led by Iris van Zelst. RFG acknowledges funding by CNES through APR project "VenusGeox". IvZ, JM, and ACP acknowledge the financial support and endorsement from the DLR Management Board Young Research Group Leader Program and the Executive Board Member for Space Research and Technology. IvZ also gratefully acknowledges the support by the Deutsche Forschungsgemeinschaft (DFG, German Research Foundation), Project-ID 263649064 – TRR 170. SPN, CMS, and QB acknowledge support from the Research Council of Norway basic research program FRIPRO through the project "Airborne Inversion of Rayleigh waves" under Contract 335903. ML acknowledges funding from the European Union's Horizon Europe research and innovation program under the Marie Skłodowska-Curie grant agreement 101110489/MuSICA-V. AG acknowledges support by the Swiss National Science Foundation Postdoc Mobility Grant P500PN_21729 and by the Jet Propulsion Laboratory, California Institute of Technology, under contract (80NM0018D0004) with the National Aeronautics and Space Administration. A.H. is funded by the UK Space Agency under grant numbers ST/W002523/1, ST/W002949/1 and ST/Y005597/1.

References

Avduevskii, V. S., Vishnevetskii, S. L., Golov, I. A., Karpeiskii, I. I., Lavrov, A. D., Likhushin, V. I., ... Pronina, N. N. (1977). Measurement of wind velocity on the surface of Venus during the operation of stations Venera 9 and Venera 10. *Cosmic Research*, *14*(5), 710–713.

Banfield, D., Spiga, A., Newman, C., Forget, F., Lemmon, M., Lorenz, R., ... Banerdt, W. B. (2020, February). The atmosphere of Mars as observed by InSight. *Nature Geoscience*, *13*(3), 190-198. doi: 10.1038/s41561-020-0534-0

Bass, H. E., & Chambers, J. P. (2001, May). Absorption of sound in the Martian atmosphere. *Acoustical Society of America Journal*, *109*(5), 2371–2371. doi: 10.1121/1.4744345

Bernauer, F., Behnen, K., Wassermann, J., Egdorf, S., Igel, H., Donner, S., ... Brokesova, J. (2021, January). Rotation, strain, and translation sensors performance tests with active seismic sources. *Sensors*, *21*(1), 264. doi: 10.3390/s21010264

Bernauer, F., Garcia, R. F., Murdoch, N., Dehant, V., Sollberger, D., Schmelzbach,

C., ... de Raucourt, S. (2020, December). Exploring planets and asteroids with 6DoF sensors: Utopia and realism. *Earth, Planets and Space*, *72*(1), 191. doi: 10.1186/s40623-020-01333-9

Bernauer, F., Wassermann, J., & Igel, H. (2020, September). Dynamic tilt correction using direct rotational motion measurements. *Seismological Research Letters*, *91*(5), 2872–2880. doi: 10.1785/0220200132

Bormann, P. (2002). *New manual of seismological observatory practice.* GeoForschungsZentrum. doi: 10.2312/GFZ.NMSOP-2_ch4

Bormann, P., & Dewey, J. W. (2012). The new IASPEI standards for determining magnitudes from digital data and their relation to classical magnitudes..

Bormann, P., Wendt, S., & DiGiacomo, D. (2013). Seismic sources and source parameters. In *New manual of seismological observatory practice 2 (nmsop2)* (pp. 1–259). Deutsches GeoForschungsZentrum GFZ. doi: 10.2312/GFZ.NMSOP-2_ch3

Brissaud, Q., Krishnamoorthy, S., Jackson, J. M., Bowman, D. C., Komjathy, A., Cutts, J. A., ... Izraelevitz, G. J., J. S. andWalsh (2021). The first detection of an earthquake from a balloon using its acoustic signature. *Geophysical Research Letters*, *48*(12). doi: 10.1029/2021gl093013

Byrne, P. K., Ghail, R. C., Şengör, A. M. C., James, P. B., Klimczak, C., & Solomon, S. C. (2021). A globally fragmented and mobile lithosphere on venus. *Proceedings of the National Academy of Sciences*, *118*(26). doi: 10.1073/pnas.2025919118

Carrasco, S., Knapmeyer-Endrun, B., Margerin, L., Xu, Z., Joshi, R., Schimmel, M., ... Banerdt, W. B. (2023, August). Constraints for the Martian crustal structure from Rayleigh waves ellipticity of large seismic events. *Geophysical Research Letters*, *50*(16), e2023GL104816. doi: 10.1029/2023GL104816

Chan, H. M., Parker, A. R., Piazza, A., & Richards, W. L. (2015). Fiber-optic sensing system: overview, development and deployment in flight at nasa. In *2015 ieee avionics and vehicle fiber-optics and photonics conference (avfop)* (pp. 71–73).

Chen, L., Neudeck, P. G., Meredith, R. D., Lukco, D., Spry, D. J., Nakley, L. M., ... Hunter, G. W. (2019). Sixty earth-day test of a prototype Pt/HTCC alumina package in a simulated Venus environment. *Journal of microelectronics and electronic packaging*, *16*(2), 78–83. doi: 10.4071/imaps.873073

Cheng, F., Chi, B., Lindsey, N. J., Dawe, T. C., & Ajo-Franklin, J. B. (2021). Utilizing distributed acoustic sensing and ocean bottom fiber optic cables for submarine structural characterization. *Scientific reports*, *11*(1), 5613. doi: 10.1038/s41598-021-84845-y

Daley, T., Miller, D., Dodds, K., Cook, P., & Freifeld, B. (2016). Field testing of modular borehole monitoring with simultaneous distributed acoustic sensing and geophone vertical seismic profiles at Citronelle, Alabama. *Geophysical Prospecting*, *64*(5), 1318–1334. doi: 10.1111/1365-2478.12324

Drilleau, M., Samuel, H., Garcia, R. F., Rivoldini, A., Perrin, C., Michaut, C., ... Banerdt, W. B. (2022, September). Marsquake locations and 1-D seismic models for Mars from InSight data. *Journal of Geophysical Research (Planets)*, *127*(9), e07067. doi: 10.1029/2021JE007067

Dumoulin, C., Tobie, G., Verhoeven, O., Rosenblatt, P., & Rambaux, N. (2017, June). Tidal constraints on the interior of Venus. *Journal of Geophysical Research (Planets)*, *122*(6), 1338–1352. doi: 10.1002/2016JE005249

Durán, C., Khan, A., Ceylan, S., Charalambous, C., Kim, D., Drilleau, M., ... Giardini, D. (2022, November). Observation of a Core-Diffracted P-Wave From a Farside Impact With Implications for the Lower-Mantle Structure of Mars. *Geophysical Research Letters*, *49*(21), e2022GL100887. doi: 10.1029/2022GL100887

Durán, C., Khan, A., Ceylan, S., Zenhäusern, G., Stähler, S., Clinton, J. F., &

Giardini, D. (2022, April). Seismology on Mars: An analysis of direct, reflected, and converted seismic body waves with implications for interior structure. *Physics of the Earth and Planetary Interiors*, *325*, 106851. doi: 10.1016/j.pepi.2022.106851

Garcia, R. F., Brissaud, Q., Rolland, L., Martin, R., Komatitsch, D., Spiga, A., ... Banerdt, B. (2017). Finite-difference modeling of acoustic and gravity wave propagation in Mars atmosphere: application to infrasounds emitted by meteor impacts. *Space Science Reviews*, *211*, 547–570. doi: 10.1007/s11214-016-0324-6

Garcia, R. F., Drossart, P., Piccioni, G., López-Valverde, M., & Occhipinti, G. (2009, March). Gravity waves in the upper atmosphere of Venus revealed by CO_2 nonlocal thermodynamic equilibrium emissions. *Journal of Geophysical Research (Planets)*, *114*, E00B32. doi: 10.1029/2008JE003073

Garcia, R. F., Klotz, A., Hertzog, A., Martin, R., Gérier, S., Kassarian, E., ... Mimoun, D. (2022, August). Infrasound from large earthquakes recorded on a network of balloons in the stratosphere. *Geophysical Research Letters*, *49*(15). doi: 10.1029/2022gl098844

Garcia, R. F., Lognonné, P. H., & Bonnin, X. (2005). Detecting atmospheric perturbations produced by Venus quakes. *Geophysical Research Letters*, *32*(16), 1–4. doi: 10.1029/2005GL023558

Garvin, J. B., Getty, S. A., Arney, G. N., Johnson, N. M., Kohler, E., Schwer, K. O., ... Zolotov, M. (2022). Revealing the mysteries of venus: The davinci mission. *The Planetary Science Journal*, *3*(5), 117. Retrieved from `http://dx.doi.org/10.3847/PSJ/ac63c2` doi: 10.3847/psj/ac63c2

Gérard, J. C., Saglam, A., Piccioni, G., Drossart, P., Cox, C., Erard, S., ... Sánchez-Lavega, A. (2008, January). Distribution of the O_2 infrared nightglow observed with VIRTIS on board Venus Express. *Geophysical Research Letters*, *35*(2), L02207. doi: 10.1029/2007GL032021

Gérard, J. C., Soret, L., Piccioni, G., & Drossart, P. (2014). Latitudinal structure of the Venus O_2 infrared airglow: A signature of small-scale dynamical processes in the upper atmosphere. *Icarus*, *236*, 92–103. doi: 10.1016/j.icarus.2014.03.028

Gilli, G., Lebonnois, S., González-Galindo, F., López-Valverde, M. A., Stolzenbach, A., Lefèvre, F., ... Lott, F. (2017). Thermal structure of the upper atmosphere of Venus simulated by a ground-to-thermosphere GCM. *Icarus*, *281*, 55–72. doi: 10.1016/j.icarus.2016.09.016

Gilli, G., Navarro, T., Lebonnois, S., Quirino, D., Silva, V., Stolzenbach, A., ... Schubert, G. (2021). Venus upper atmosphere revealed by a GCM: II. Model validation with temperature and density measurements. *Icarus*, *366*, 114432. doi: 10.1016/j.icarus.2021.114432

Glass, D. E., Jones, J.-P., Shevade, A. V., Bhakta, D., Raub, E., Sim, R., & Bugga, R. V. (2020). High temperature primary battery for Venus surface missions. *Journal of Power Sources*, *449*, 227492. doi: 10.1016/j.jpowsour.2019.227492

Gudkova, T. V., & Zharkov, V. N. (2020, March). Models of the internal structure of the Earth-like Venus. *Solar System Research*, *54*(1), 20–27. doi: 10.1134/S0038094620010049

Gülcher, A. J. P., Gerya, T. V., Montési, L. G. J., & Munch, J. (2020). Corona structures driven by plume–lithosphere interactions and evidence for ongoing plume activity on Venus. *Nature Geoscience*, *13*(8), 547–554. doi: 10.1038/s41561-020-0606-1

Heracle. (2023, 11). *Step Index Multimode Fibers Metal Coated Series: Gold.* Retrieved from `https://www.heracle.de/products/step-index-multimode-fibers-metal-coated-series-gold/?lang=en`

Herrick, R., & Hensley, S. (2023). Surface changes observed on a Venusian volcano during the Magellan mission. *Science*, *379*(6638), 1205–1208. doi: 10.1126/

763 science.abm7735
764 Hudson, T. S., Baird, A. F., Kendall, J.-M., Kufner, S.-K., Brisbourne, A. M.,
765 Smith, A. M., ... Clarke, A. (2021). Distributed acoustic sensing (DAS)
766 for natural microseismicity studies: A case study from Antarctica. *Journal of*
767 *Geophysical Research: Solid Earth*, *126*(7), e2020JB021493.
768 Hunter, G., Kremic, T., & Neudeck, P. G. (2021). High temperature electron-
769 ics for Venus surface applications: A summary of recent technical advances.
770 In *Bulletin of the american astronomical society* (Vol. 53, p. 399). doi:
771 10.3847/25c2cfeb.e3883e19
772 Jacobsen, W., Soufiane, A., & D'Urso, J. (2018). 500° c-rated optical fibers for high
773 temperature applications. In *80th eage conference and exhibition 2018* (Vol.
774 2018, pp. 1–5).
775 Jousset, P., Currenti, G., Schwarz, B., Chalari, A., Tilmann, F., Reinsch, T.,
776 ... Krawczyk, C. M. (2022). Fibre optic distributed acoustic sensing
777 of volcanic events. *Nature communications*, *13*(1), 1753. doi: 10.1038/
778 s41467-022-29184-w
779 Kerzhanovich, V. V., & Marov, M. I. (1983). The atmospheric dynamics of Venus
780 according to Doppler measurements by the Venera entry probes. In *Venus* (pp.
781 766–778). The University of Arizona Press.
782 Kim, D., Banerdt, W. B., Ceylan, S., Giardini, D., Lekić, V., Lognonné, P., ... Pan-
783 ning, M. P. (2022, October). Surface waves and crustal structure on Mars.
784 *Science*, *378*(6618), 417–421. doi: 10.1126/science.abq7157
785 Klaasen, S., Paitz, P., Lindner, N., Dettmer, J., & Fichtner, A. (2021). Dis-
786 tributed acoustic sensing in volcano-glacial environments—Mount Meager,
787 British Columbia. *Journal of Geophysical Research: Solid Earth*, *126*(11),
788 e2021JB022358. doi: 10.1029/2021JB022358
789 Klaasen, S., Thrastarson, S., Çubuk-Sabuncu, Y., Jónsdóttir, K., Gebraad, L.,
790 Paitz, P., & Fichtner, A. (2023). Subglacial volcano monitoring with
791 fibre-optic sensing: Grímsvötn, Iceland. *Volcanica*, *6*(2), 301–311. doi:
792 10.30909/vol.06.02.301311
793 Kremic, T., Ghail, R., Gilmore, M., Hunter, G., Kiefer, W., Limaye, S., ... Wilson,
794 C. (2020). Long-duration Venus lander for seismic and atmospheric science.
795 *Planetary Space Science*, *190*, 104961. doi: 10.1016/j.pss.2020.104961
796 Krishnamoorthy, S., & Bowman, D. C. (2023, January). A "Floatilla" of Airborne
797 Seismometers for Venus. *Geophysical Research Letters*, *50*(2), e2022GL100978.
798 doi: 10.1029/2022GL100978
799 Ksanfomaliti, L. V., Goroshkova, N. V., & Khondyrev, V. K. (1983). Wind velocity
800 on the Venus surface from acoustic measurements. *Kosmicheskie Issledovaniia*,
801 *21*, 218–224.
802 Ksanfomaliti, L. V., Zubkova, V. M., Morozov, N. A., & Petrova, N. A. (1982). Mi-
803 croseisms at the Venera 13 and Venera 14 landing sites. *Pisma v Astronomich-*
804 *eskii Zhurnal*, *8*, 444–447.
805 Lebonnois, S., Schubert, G., Forget, F., & Spiga, A. (2018, November). Planetary
806 boundary layer and slope winds on Venus. *Icarus*, *314*, 149–158. doi: 10.1016/
807 j.icarus.2018.06.006
808 Lefèvre, M. (2022). Venus boundary layer dynamics: Eolian transport and convec-
809 tive vortex. *Icarus*, *387*, 115167. doi: 10.1016/j.icarus.2022.115167
810 Lefèvre, M., Spiga, A., Lebonnois, S., & Forget, F. (2024). Control of the surface
811 temperature on Venus by slope winds. *To be Submitted*.
812 Lindsey, N. J., & Martin, E. R. (2021). Fiber-optic seismology. *Annual Review*
813 *of Earth and Planetary Sciences*, *49*, 309–336. doi: 10.1146/annurev-earth
814 -072420-065213
815 Lior, I., Sladen, A., Rivet, D., Ampuero, J.-P., Hello, Y., Becerril, C., ... others
816 (2021). On the detection capabilities of underwater distributed acoustic sens-
817 ing. *Journal of Geophysical Research: Solid Earth*, *126*(3), e2020JB020925.

Lognonné, P., Banerdt, W. B., Clinton, J., Garcia, R. F., Giardini, D., Knapmeyer-Endrun, B., ... Pike, W. T. (2023, May). Mars seismology. *Annual Review of Earth and Planetary Sciences*, *51*, 643–670. doi: 10.1146/annurev-earth-031621-073318

Lognonné, P., Banerdt, W. B., Giardini, D., Pike, W. T., Christensen, U., Laudet, P., ... Wookey, J. (2019, January). SEIS: Insight's seismic experiment for internal structure of Mars. *Space Science Reviews*, *215*(1), 12. doi: 10.1007/s11214-018-0574-6

Lognonné, P., Karakostas, F., Rolland, L., & Nishikawa, Y. (2016, August). Modeling of atmospheric-coupled Rayleigh waves on planets with atmosphere: From Earth observation to Mars and Venus perspectives. *The Journal of the Acoustical Society of America*, *140*(2), 1447–1468. doi: 10.1121/1.4960788

López-Valverde, M. A., López-Puertas, M., Funke, B., Gilli, G., Garcia-Comas, M., Drossart, P., ... Formisano, V. (2011, August). Modeling the atmospheric limb emission of CO_2 at 4.3 μm in the terrestrial planets. *Planetary and Space Science*, *59*(10), 988–998. doi: 10.1016/j.pss.2010.02.001

Lorenz, R. D. (2012). Planetary seismology—expectations for lander and wind noise with application to Venus. *Planetary and Space Science*, *62*(1), 86–96. doi: 10.1016/j.pss.2011.12.010

Lorenz, R. D. (2016). Surface winds on Venus: Probability distribution from in-situ measurements. *Icarus*, *264*, 311–315. doi: 10.1016/j.icarus.2015.09.036

Lorenz, R. D., & Panning, M. P. (2018). Empirical recurrence rates for ground motion signals on planetary surfaces. *Icarus*, *303*, 273–279. doi: 10.1016/j.icarus.2017.10.008

Makela, J. J., Lognonné, P., Hébert, H., Gehrels, T., Rolland, L., Allgeyer, S., ... Lamouroux, J. (2011, July). Imaging and modeling the ionospheric airglow response over Hawaii to the tsunami generated by the Tohoku earthquake of 11 March 2011. *Geophysical Research Letters*, *38*(13), L00G02. doi: 10.1029/2011GL047860

Margot, J.-L., Campbell, D. B., Giorgini, J. D., Jao, J. S., Snedeker, L. G., Ghigo, F. D., & Bonsall, A. (2021). Spin state and moment of inertia of venus. *Nature Astronomy*, *5*(7), 676–683. Retrieved from `http://dx.doi.org/10.1038/s41550-021-01339-7` doi: 10.1038/s41550-021-01339-7

Martinez, A., Lebonnois, S., Millour, E., Pierron, T., Moisan, E., Gilli, G., & Lefèvre, F. (2023). Exploring the variability of the venusian thermosphere with the IPSL Venus GCM. *Icarus*, *389*, 115272. doi: 10.1016/j.icarus.2022.115272

Mimoun, D., Murdoch, N., Lognonné, P., Hurst, K., Pike, W. T., Hurley, J., ... Banerdt, W. B. (2017, October). The noise model of the SEIS seismometer of the InSight mission to Mars. *Space Science Reviews*, *211*(1–4), 383–428. doi: 10.1007/s11214-017-0409-x

Moroz, V. I. (1983). Summary of preliminary results of the Venera 13 and Venera 14 missions. In *Venus* (pp. 45–68). The University of Arizona Press.

Nachman, A. I., Smith III, J. F., & Waag, R. C. (1990). An equation for acoustic propagation in inhomogeneous media with relaxation losses. *The Journal of the Acoustical Society of America*, *88*(3), 1584–1595. doi: 10.1121/1.400317

Näsholm, S. P., Iranpour, K., Wuestefeld, A., Dando, B. D., Baird, A. F., & Oye, V. (2022). Array signal processing on distributed acoustic sensing data: Directivity effects in slowness space. *Journal of Geophysical Research: Solid Earth*, *127*(2), e2021JB023587. doi: 10.1029/2021JB023587

Neudeck, P. G., Spry, D. J., Krasowski, M. J., Prokop, N. F., Beheim, G. M., Chen, L.-Y., & Chang, C. W. (2018). Year-long 500° C operational demonstration of up-scaled 4H-SiC JFET integrated circuits. *Journal of Microelectronics and Electronic Packaging*, *15*(4), 163–170.

Noe, S., Yuan, S., Montagner, J. P., & Igel, H. (2022, May). Anisotropic elastic parameter estimation from multicomponent ground-motion observations: a

theoretical study. *Geophysical Journal International*, *229*(2), 1462–1473. doi: 10.1093/gji/ggac006

Occhipinti, G., Coïsson, P., Makela, J. J., Allgeyer, S., Kherani, A., Hebert, H., & Lognonné, P. (2011, July). Three-dimensional numerical modeling of tsunami-related internal gravity waves in the Hawaiian atmosphere. *Earth, Planets and Space*, *63*(7), 847–851. doi: 10.5047/eps.2011.06.051

Parker, A. R., Chan, H. M., Lopez-Zepeda, J., & Schallhorn, P. A. (2024). Design, fabrication, testing and validation of a ruggedized fiber optics sensing system (foss) for launch application. In *Aiaa scitech 2024 forum* (p. 2268).

Petculescu, A. (2016). Acoustic properties in the low and middle atmospheres of mars and venus. *The Journal of the Acoustical Society of America*, *140*(2), 1439–1446. doi: https://doi.org/10.1121/1.4960784

Peterson, J. (1993). *Observation and modeling of background seismic noise.* U.S. Geol. Surv. Open-File Rept. 92-322. Albuquerque.

Reinsch, T., & Henninges, J. (2010). Temperature-dependent characterization of optical fibres for distributed temperature sensing in hot geothermal wells. *Measurement Science and Technology*, *21*(9), 094022.

Samuel, H., Drilleau, M., Rivoldini, A., Xu, Z., Huang, Q., Garcia, R. F., ... Banerdt, W. B. (2023, October). Geophysical evidence for an enriched molten silicate layer above Mars's core. *Nature*, *622*(7984), 712–717. doi: 10.1038/s41586-023-06601-8

Schmelzbach, C., Donner, S., Igel, H., Sollberger, D., Taufiqurrahman, T., Bernauer, F., ... Robertsson, J. (2018, May). Advances in 6C seismology: Applications of combined translational and rotational motion measurements in global and exploration seismology. *Geophysics*, *83*(3), WC53–WC69. doi: 10.1190/geo2017-0492.1

Seiff, A., & Kirk, D. B. (1991). Waves in Venus' middle and upper atmosphere; Implication of Pioneer Venus probe data above the clouds. *Journal of Geophysical Research*, *96*(A7), 11021–11032. doi: 10.1029/91JA01101

Smrekar, S., Hensley, S., Nybakken, R., Wallace, M., Perkovic-Martin, D., You, T.-H., ... Mazarico, E. (2022). VERITAS (Venus Emissivity, Radio Science, InSAR, Topography, and Spectroscopy): A discovery mission. In *2022 ieee aerospace conference (aero).* IEEE. Retrieved from `http://dx.doi.org/10.1109/aero53065.2022.9843269` doi: 10.1109/aero53065.2022.9843269

Smrekar, S. E., Ostberg, C., & O'Rourke, J. G. (2023). Earth-like lithospheric thickness and heat flow on Venus consistent with active rifting. *Nature Geoscience*, *16*(1), 13–18. doi: 10.1038/s41561-022-01068-0

Smrekar, S. E., Stofan, E. R., Mueller, N., Treiman, A., Elkins-Tanton, L., Helbert, J., ... Drossart, P. (2010). Recent hotspot volcanism on Venus from VIRTIS emissivity data. *Science*, *328*(5978), 605–608. doi: 10.1126/science.1186785

Sollberger, D., Bradley, N., Edme, P., & Robertsson, J. O. A. (2023, July). Efficient wave type fingerprinting and filtering by six-component polarization analysis. *Geophysical Journal International*, *234*(1), 25–39. doi: 10.1093/gji/ggad071

Stähler, S. C., Khan, A., Banerdt, W. B., Lognonné, P., Giardini, D., Ceylan, S., ... Smrekar, S. E. (2021, July). Seismic detection of the martian core. *Science*, *373*(6553), 443–448. doi: 10.1126/science.abi7730

Stevenson, D., Cutts, J., MimounDavid, Arrowsmith, S., Banerdt, B., Blom, P., ... Tsai, V. (2015, April). *Probing the interior structure of Venus* (Tech. Rep.). Keck Institute for Space Studies: Venus Seismology Study Team.

Stolov, A., & OFS. (2019, 1). *Testing Optical Fiber: Undersea and Downhole Applications.* Retrieved from `https://www.photonics.com/Articles/Testing_Optical_Fiber_Undersea_and_Downhole/p5/v170/i1115/a64288`

Surkov, Y. A., Barsukov, V., Moskalyeva, L., Kharyukova, V., & Kemurdzhian, A. (1984). New data on the composition, structure, and properties of Venus rock obtained by Venera 13 and Venera 14. *Journal of Geophysical Research: Solid*

Earth, *89*(S02), B393–B402.

Sutin, B. M., Cutts, J., Didion, A. M., Drilleau, M., Grawe, M., Helbert, J., ... Wallace, M. (2018, July). VAMOS: a SmallSat mission concept for remote sensing of Venusian seismic activity from orbit. In M. Lystrup, H. A. MacEwen, G. G. Fazio, N. Batalha, N. Siegler, & E. C. Tong (Eds.), *Space telescopes and instrumentation 2018: Optical, infrared, and millimeter wave* (Vol. 10698, p. 106985T). doi: 10.1117/12.2309439

Tian, Y., Herrick, R. R., West, M. E., & Kremic, T. (2023). Mitigating Power and Memory Constraints on a Venusian Seismometer. *Seismological Research Letters*, *94*(1), 159–171. doi: 10.1785/0220220085

Trahan, A. J., & Petculescu, A. (2020). Absorption of infrasound in the lower and middle clouds of Venus. *The Journal of the Acoustical Society of America*, *148*(1), 141–152. doi: 10.1121/10.0001520

Van Zelst, I. (2022). Comment on "Estimates on the frequency of volcanic eruptions on Venus" by Byrne & Krishnamoorthy (2022). *Journal of Geophysical Research: Planets*, *127*(12), e2022JE007448. doi: 10.1029/2022JE007448

Van Zelst, I., Maia, J., Plesa, A.-C., Ghail, R., & Spühler, M. (2024). Estimates on the possible annual seismicity of Venus [preprint]. *EarthArXiv*. doi: 10.31223/X5DQ0C

Walter, F., Gräff, D., Lindner, F., Paitz, P., Köpfli, M., Chmiel, M., & Fichtner, A. (2020). Distributed acoustic sensing of microseismic sources and wave propagation in glaciated terrain. *Nature communications*, *11*(1), 2436. doi: 10.1038/s41467-020-15824-6

Wang, H. F., Zeng, X., Miller, D. E., Fratta, D., Feigl, K. L., Thurber, C. H., & Mellors, R. J. (2018). Ground motion response to an ML 4.3 earthquake using co-located distributed acoustic sensing and seismometer arrays. *Geophysical Journal International*, *213*(3), 2020–2036. doi: 10.1093/gji/ggy102

Widemann, T., Straume-Lindner, A. G., Ocampo, A., Voirin, T., Carter, L., Hensley, S., ... Dumoulin, C. (2022). EnVision: a nominal science phase spanning six Venus sidereal days (four earth years). In *Agu fall meeting abstracts* (Vol. 2022, pp. P55B–05).

Wilson, C. F., Zetterling, C.-M., & Pike, W. T. (2016). Venus long-life surface package. White paper submitted in response to ESA's call for new scientific ideas. *arXiv e-prints*, arXiv:1611.03365. doi: 10.48550/arXiv.1611.03365

Xu, Z., Broquet, A., Fuji, N., Kawamura, T., Lognonné, P., Montagner, J.-P., ... Banerdt, W. B. (2023, April). Investigation of Martian regional crustal structure near the dichotomy using S1222a surface-wave group velocities. *Geophysical Research Letters*, *50*(8), e2023GL103136. doi: 10.1029/2023GL103136

Zhan, Z. (2020). Distributed acoustic sensing turns fiber-optic cables into sensitive seismic antennas. *Seismological Research Letters*, *91*(1), 1–15. doi: 10.1785/0220190112

Zharkov, V. N. (1983, October). Models of the internal structure of Venus. *Moon and Planets*, *29*(2), 139–175. doi: 10.1007/BF00928322